● RESEARCH ARTICLE

A progressive compression model of thoracic spinal cord injury in mice: function assessment and pathological changes in spinal cord

Guo-dong Sun[1, #], Yan Chen[1, #], Zhi-gang Zhou[1], Shu-xian Yang[2], Cheng Zhong[3], Zhi-zhong Li[1, 4, *]

1 Department of Orthopedics, First Affiliated Hospital, Jinan University, Guangzhou, Guangdong Province, China
2 Biomedical Translational Research Institute and Guangdong Province Key Laboratory of Molecular Immunology and Antibody Engineering, Jinan University, Guangzhou, Guangdong Province, China
3 Department of Traumatology and Plastic Surgery, The Affiliated Jiangmen Traditional Chinese Medicine Hospital of Jinan University, Jiangmen, Guangdong Province, China
4 Department of Orthopedics, Heyuan People's Hospital (Heyuan Affiliated Hospital of Jinan University), Heyuan, Guangdong Province, China

Graphical Abstract

Establishment of a mouse model of thoracic spinal cord progressive compression
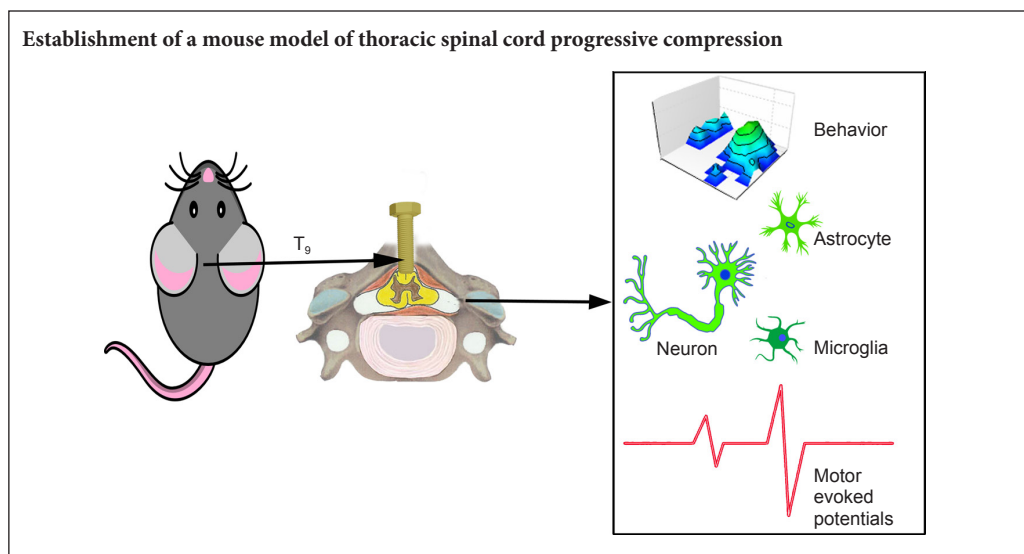
Correspondence to:
Zhi-zhong Li, Ph.D.,
lizhizhongjd@163.com.

#*These authors contributed equally to this study.*

orcid:
0000-0002-2306-7633
(Zhi-zhong Li)

Abstract

Non-traumatic injury accounts for approximately half of clinical spinal cord injury, including chronic spinal cord compression. However, previous rodent spinal cord compression models are mainly designed for rats, few are available for mice. Our aim is to develop a thoracic progressive compression mice model of spinal cord injury. In this study, adult wild-type C57BL/6 mice were divided into two groups: in the surgery group, a screw was inserted at T_9 lamina to compress the spinal cord, and the compression was increased by turning it further into the canal (0.2 mm) post-surgery every 2 weeks up to 8 weeks. In the control group, a hole was drilled into the lamina without inserting a screw. The results showed that Basso Mouse Scale scores were lower and gait worsened. In addition, the degree of hindlimb dysfunction in mice was consistent with the degree of spinal cord compression. The number of motor neurons in the anterior horn of the spinal cord was reduced in all groups of mice, whereas astrocytes and microglia were gradually activated and proliferated. In conclusion, this progressive compression of thoracic spinal cord injury in mice is a preferable model for chronic progressive spinal cord compression injury.

Key Words: nerve regeneration; progressive spinal cord compression injury; pathological changes; Basso Mouse Scale scores; gait; motor evoked potentials; astrocytes; microglia; motor neurons; hindlimb dysfunction; neural regeneration

Introduction

Animal models of spinal cord injury (SCI) can be useful to understand the pathophysiological progress and test potential therapies (Young, 2002; Cheriyan et al., 2014). Nevertheless, chronic progressive spinal stenosis caused by epidural spinal cord compression is very common clinically, accounting for 30–80% of non-traumatic SCI (Chagas et al., 2005; Uchida et al., 2005; Scivoletto et al., 2014). Compression can be caused by degeneration, tumor, tuberculosis, and hematoma (Manabe et al., 1988; Rajah et al., 2014; Fonseca et al., 2016; Rades et al., 2016; Tatsui et al., 2016; Watanabe et al., 2016). The precise pathophysiological mechanisms of chronic spinal cord compression remain poorly understood, but circulatory insufficiency leading to ischemia has been suggested as a possible contributor to neural degeneration (Karadimas et al., 2010; Kalsi-Ryan et al., 2013). Compression models of SCI can be established by reducing the diameter of spinal canal (Ziu et al., 2014), implanting polymers (Karadimas et al., 2013) or placing spacers in the epidural space (Dimar et al., 1999). Alternatively, epidural spinal cord compression can be achieved using calibrated clips (Nashmi and Fehlings, 2001; Weaver et al., 2001; Fehlings, 2009) or placing a specific weight in the epidural space (Perdiki et al., 1998; Li et al., 2004). However, most of these methods mimic compression acutely but not chronically. Most of the aforementioned models were designed for rats, and mouse compression models are rarely reported. Since transgenic mouse lines are much more abundant than transgenic rat lines, the establishment of mouse models is important for studies on the genetic or molecular mechanisms of SCI.

Therefore, the present study aims to establish a mouse model of chronic progressive spinal cord compression and evaluate its efficacy and the pattern between progressive hindlimb motor dysfunction and spinal cord histopathology based on behavioral and histopathological changes.

Materials and Methods

Animals and groups

A total of 48 adult healthy wild type female C57BL/6 mice weighing 20–25 g, aged 8 weeks were provided by the Guangdong Experimental Animal Center in China (license No. 11401300044788), and this study was approved by Animal Ethics Committee of Jinan University of China (approval No. 20162302023).

Animals were randomly divided into a control group ($n = 12$) and an experimental surgery group ($n = 36$). The surgery group was further subdivided into six groups (2-, 4-, 6-, 8-, 10-, and 12-week subgroups; $n = 6$), according to the length of time of screw insertion.

Each group of mice was housed in a separate cage, had free access to water and normal diet, in a room at 20–25°C and relative humidity of 60%.

Preparation of progressive compression models of SCI

Customized stainless steel flat-head miniscrews and matching nuts were made according to a previous study (Hautier et al., 2014). The thickness of the lamina near the spinous

process in mice was 0.23 ± 0.01 mm; the sagittal diameter of the T_9 vertebral canal was 1.37 ± 0.05 mm, and the transverse diameter was 1.70 ± 0.05 mm. Customized flat-head stainless steel miniscrew diameter 1.2 mm, pitch 0.2 mm, thread length 2.5 mm, and the thickness of matching bolt was 1 mm. All implants were customized and purchased from Huayi Metal (Dongguan, China).

Mice were anesthetized by intraperitoneal injection of 0.02 mL/g 1.25% tribromoethanol (Avertin, Sigma, Guangzhou, China), followed by skin preparation. Each mouse was placed in prone position, and a 1 mL preoperative dose of gentamicin (800 U/mL; Succhi Pharmaceutical, Zhongshan, China) was administered subcutaneously. Following disinfection with povidone iodine (Likang, Shanghai, China), an incision was made along the highest point of the spine (level of T_9). The paraspinous muscles were stripped off and the lamina of T_9 was completely exposed. The spine was stabilized with a spinal fixator at T_9 and a 1-mm diameter flat-head drill bit was used for vertical drilling near spinous process. Care was taken to avoid drilling through the inner cortical layer of the lamina. The stabilizing nut was affixed to the lamina using glass ionomer cement. The minibolt was screwed in seven turns and entered the spinal canal (**Additional Figure 1**). Responses of the hindlimbs of mice were observed. If the hindlimbs became rigid, the tail was flicked or any other acute sign of SCI occurred when the bolt was being screwed in, the animal was excluded from the experiment; otherwise, implantation of the screw was considered successful. The muscles were then tightly sutured, leaving the nut of the flathead miniscrew subcutaneous, and the skin was sutured. Mice in the control group only received an incision to expose the T_9 lamina and a drilled hole, without insertion of any screws. All mice in each group received a subcutaneous injection of 1 mL gentamicin (800 U/mL) for 3 days post-surgery. After surgery, the animals were placed on a heating pad (37°C) during recovery, they were then observed and fed as before. Voiding and bladder filling were checked regularly twice a day.

Every 2 weeks for 2 months after the surgical procedure, based on different time points (which also refer to different progressive compression degree respectively), the skin of each mouse in the surgery subgroups was re-incised and the nut exposed and given one more turn into the canal (0.2 mm). At each turn of the screw, mice of each group received a subcutaneous injection of 1 mL gentamicin (800 U/mL) for 3 days, and were housed and fed as aforementioned. Throughout the study, if an animal died, or if severe infection or a loose screw were observed, the affected animals were excluded and immediately replaced.

Motor function evaluation

Basso Mouse Scale (BMS) scoring, EthoVision-assisted open-field testing, and CatWalk-assisted gait analyses were conducted at 2, 4, 6, 8, 10, and 12 weeks after surgery.

BMS scoring

BMS primary scoring system is based on a scale that ranges

from 0 (complete paralysis) to 9 points (completely normal) (Basso et al., 2006). The mice were placed on a flat surface and observed for 5 minutes. Hindlimb motor function was scored using the single-blind method by two independent, blinded observers. The mean score of both observers for the two hindlimbs was used as the BMS of the sample.

EthoVision-assisted open-field test
Mice were placed under illumination (500 lux) in one corner of a 50 cm × 50 cm × 35 cm experimental box. The trajectories of mice were recorded for 15 minutes. Six mice from each group were continuously monitored. The XT 7.0 Etho-Vision video-tracking system (Noldus, Wageningen, Netherlands) was used to analyze trajectories and total distance (Noldus et al., 2001).

CatWalk-assisted gait analysis
Gait analysis of mice from each group was conducted using the CatWalk XT video-assisted automated quantitative gait analysis system (Noldus). Each mouse was subjected to at least three assessments, each of which required continuous walking on a glass plate along a 50 cm path. The entire experiment was conducted in a dark, quiet environment. The CatWalk system automatically identified and tagged each paw print, then generated a series of parameters including: (1) paw print statistics (print length, print width, maximum contact area, mean intensity, stride length, swing, and swing speed); (2) general parameters (average speed and cadence); (3) step sequence parameters; and (4) base of support (Hamers et al., 2006; Neumann et al., 2009).

Motor-evoked potentials
To evaluate SCI recovery, the motor evoked potentials were assayed by electromyography at control, 4, 8, and 12 weeks following the previously described methods (Ding et al., 2014). First, the mice were anesthetized using 1.25% tribromoethanol (3.0 mL/kg). Then, a stimulating electrode was applied to the rostral ends of the surgical spinal cord. The recording electrode was placed in the biceps flexor cruris. The ground electrode was placed on the tail. A single square wave stimulus (0.5 ms, 1 Hz and 0.5 mA), with a 2-ms time delay, was used. The amplitude was measured from the initiation point of the first response wave to its highest point. Peak-to-peak amplitude was used to detect the nerve conduction function in the hindlimb of mice. All potentials were amplified and recorded using a digital oscilloscope RM6240BD (Chengdu Instrument Factory, Chengdu, China).

Histological and pathological observation
Spinal cord specimens were acquired from sacrificed animals of the surgical group respectively at 2, 4, 6, 8, 10, and 12 weeks after screw implantation, while those of the control group taken at day 1 post-surgery. Mice were anesthetized by intraperitoneal injection of 1.25% tribromoethanol (0.02 mL/g body weight). Following thoracotomy, the left ventricle was rapidly perfused with 50 mL of normal saline and then perfused with 30 mL 4% paraformaldehyde for fixation. A spinal cord segment (4 mm in length) was resected from the level of T_9 and fixed in 4% paraformaldehyde for 24 hours, then transferred into 30% sucrose solution until the tissue sank. After freezing, the tissues were cut into 15 μm sections. Nissl staining with 0.1% cresyl violet was used to visualize the density and distribution of neurons and glia.

For immunofluorescence, slices were incubated with the following primary antibodies: rabbit anti-mouse ionized calcium-binding adapter molecule 1 (Iba-1) (1:1,000; Abcam, Guangzhou, China) which was up-regulated in microglia following nerve injury (Li et al., 2014), rabbit anti-mouse glial fibrillary acidic protein (GFAP) (1:1,500; Abcam), expressed in the central nervous system in astrocytes (Hol and Pekny, 2015), and goat anti-mouse choline acetyltransferase (ChAT) (1:500; Millipore, Darmstadt, Germany), an immunohistochemical marker for motor neurons in central nervous system (Han et al., 2015) incubated for 12 hours at 4°C. Fluorescent Alexa Fluor488 horse anti-rabbit and horse anti-goat secondary antibodies (1:1,000; Invitrogen, CA, USA) were used for visualization after 60 minutes at 37°C. An inverted fluorescence microscope (Leica DM6000, Wetzlar, Germany) was used to capture images and conduct further analysis. To determine the total number of neurons, the number of ChAT$^+$ motor neurons in both spinal cord anterior horns was estimated. Iba1 and GFAP staining was conducted for the morphology and activation of microglia and astrocytes respectively (Han et al., 2015).

Statistical analysis
Data were processed and analyzed with the SPSS 19.0 statistical software (IBM, Armork, New York, USA) and presented as mean ± SD. One-way analysis of variance was used to compare the BMS scores, the EthoVision-assisted behavioral test, CatWalk-assisted gait analysis results, Motor evoked potentials, peak-to-peak amplitude and ChAT$^+$ motor neuron counts among the groups. The Student-Newman-Keuls test was used for further comparisons between two groups. $P < 0.05$ was considered to be statistically significant.

Results
Motor function change in progressive compression models of SCI
BMS scoring
Control mice scored 9 points and demonstrated good hindlimb motor function. In the experimental groups BMS declined gradually from 8.60 ± 0.22 at 2 weeks to 4.00 ± 0.39 at 12 weeks (**Figure 1**), as compression of the screw was increased. In addition to the 2-week group and BMS assessment 1 day post-surgery, BMS scores of the other experimental groups at 6, 8, 10 and 12 weeks were significantly lower than those of the control group ($P < 0.0001$); significant differences were also noted between the control (assessed 1 day post-surgery) and 4-week group ($P < 0.05$); the 4- and 8-week groups ($P < 0.0001$); and the 8- and 12-week groups ($P < 0.0001$).
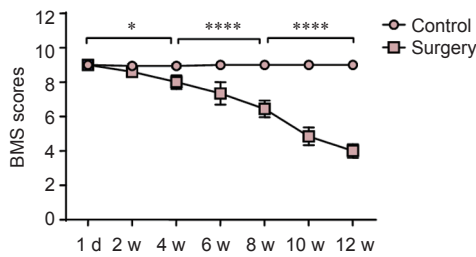
Figure 1 Change of Basso Mouse Scale (BMS) scores in progressive compression models of spinal cord injury.
Mice with low BMS scores had poorer hindlimb function. The two weekly BMS of the six mice in the control group scored 9 points throughout the 12 weeks post-surgery. In surgery groups, as compression increased, BMS declined gradually. Data are expressed as the mean ± SD (n = 6 mice per group), and analyzed by one-way analysis of variance. *$P < 0.05$, ****$P < 0.0001$, *vs.* control group. Control group: Did not receive the screw injury; surgery group: progressive spinal cord compression injury. d: Day; w: weeks.
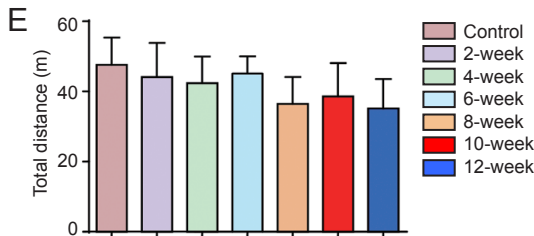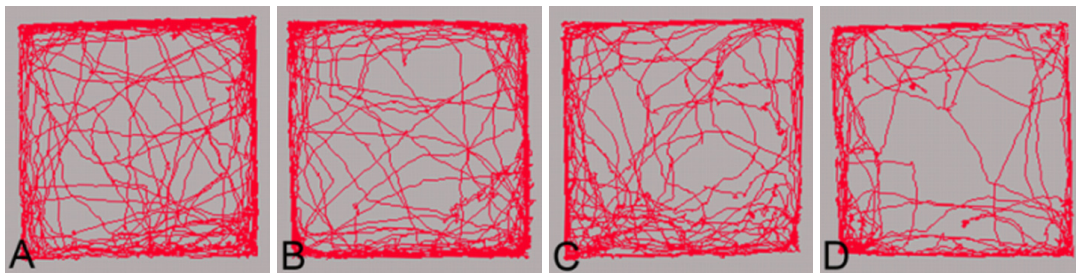
Figure 2 Change of EthoVision-assisted Open-field test in progressive compression models of spinal cord injury.
(A–D) The trajectories were indicated with red lines in the control, 4-week, 8-week, and 12-week groups, respectively. The trajectories of open field actually declined slightly but without significant difference. (E) The total distance in 15 minutes. Data are expressed as the mean ± SD (n = 6 mice per group), and analyzed by one-way analysis of variance. Control group: Mice did not receive the injury; 2-, 4-, 6-, 8-, 10-, 12-week groups: after 2, 4, 6, 8, 10, 12 weeks of progressive spinal cord compression injury.
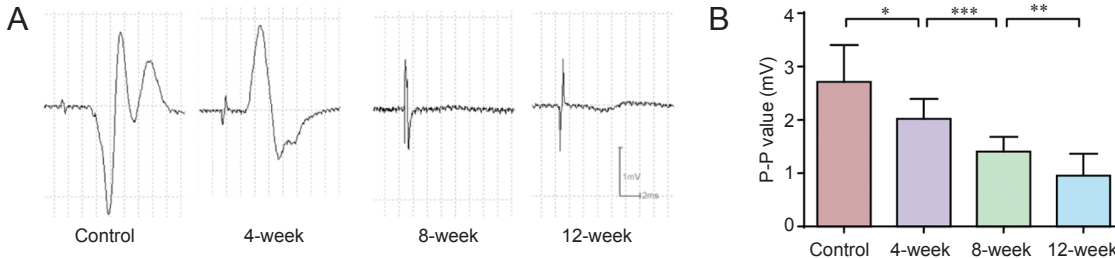
Figure 4 Change of motor evoked potentials in progressive compression models of spinal cord injury.
Peak-to-peak amplitude (P-P value) was used to detect the nerve conduction function in the hindlimb of mice. Data are expressed as the mean ± SD (n = 6 mice per group), and analyzed by Student-Newman-Keuls test. *$P < 0.05$, **$P < 0.01$, ***$P < 0.001$. Control group: Mice did not receive the injury; 4-, 8-, 12-week group: after 4, 8, 12 weeks of progressive spinal cord compression injury.
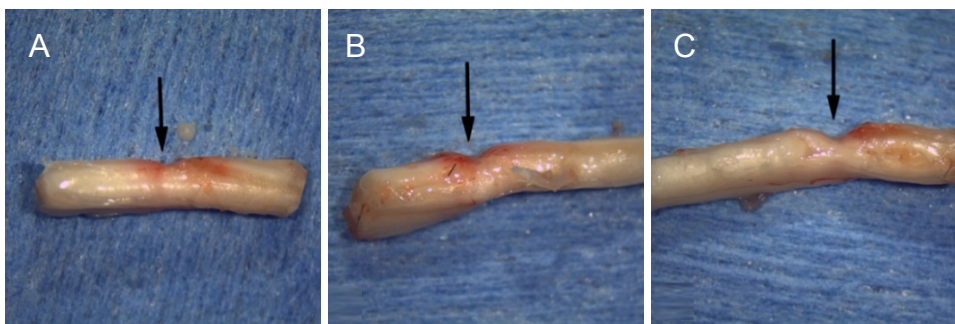
Figure 5 Change of spinal cord gross morphology in progressive compression models of spinal cord injury.
Black arrows point to the dura mater beneath drilling site of lamina in control group (A); whereas those in 4-week (B) and 8-week (C) groups are increasingly concave, suggesting the oppression point. Control group: Mice did not receive the injury; 4-, 8-week groups: after 4, 8 weeks of progressive spinal cord compression injury.

EthoVision-assisted open-field test
Figure 2 shows that mice from both the control and surgery groups preferred to move around the periphery of the open field, and occasionally crossed the central area. The total distance of travel by controls was 47.57 ± 7.73 m. Although the total distance declined from 44.07 ± 9.77 m in the 2-week group to 35.14 ± 8.38 m in the 12-week group there were no significant differences between the groups ($P > 0.05$).

CatWalk-assisted gait analysis
The maximum contact areas and paw print lengths gradually declined and were significantly shorter compared to control

0.05). Although the print width and the swing speed of hind paws in the surgery groups were generally less than those in the control group (swing speed from 32.51 ± 8.21 cm/s at 2 weeks to 12.24 ± 8.11 cm/s at 12 weeks, right hindlimbs print width from 0.63 ± 0.09 cm at 2 weeks to 0.29 ± 0.28 cm at 12 weeks) no other patterns were observed (**Figure 3C**, **F**). The average speed of mice of the control group compared to that at each interval or group exhibited a downtrend with aggravating compression with time from 17.37 ± 2.00 cm/s at 2 weeks to 4.35 ± 1.80 cm/s at 12 weeks (**Figure 3H**). Although from 6 weeks onward, this change was mitigated. Significant differences were noted between the control and 2-week groups ($P < 0.01$), the 2- and 4-week groups ($P < 0.01$), and the 4- and 8-week groups ($P < 0.05$).

Cadence in each group was also reduced with increasing spinal cord compression from 11.94 ± 2.30 steps/s at 2 weeks to 5.24 ± 1.16 steps/s at 12 weeks (**Figure 3I**), and significant differences were noted between the control and 4-week groups and the 8- and 12-week groups ($P < 0.01$, $P < 0.05$, respectively); whereas a plateau was noted between the 4- and 8-week groups. The step sequence (**Figure 3J**) data captured by the CatWalk gait analysis system at 10 and 12 weeks post-surgery were poor or missing, since mice of the surgery groups showed a significant decline in spontaneous activity and hindlimb locomotor activity. Therefore, these groups were excluded in the statistical analysis. The regular step sequences of normal mice declined from $67.01 \pm 10.24\%$ in the control group to $46.27 \pm 24.02\%$ in the 8-week group; however, no significant differences were noted in other step sequences. The base of support of hindlimbs first increased with increasing aggravation of compression from 1.87 ± 0.13 cm in the control group to 2.55 ± 0.28 cm in 4-week group ($P < 0.05$), and then to 3.42 ± 0.26 cm in the 8-week group ($P < 0.01$); however, this was later reduced to 1.99 ± 0.60 cm in the 12-week group ($P < 0.01$) (**Figure 3K**).

Motor evoked potentials in progressive compression models of SCI
As expected, the amplitude (peak-to-peak amplitude) of motor evoked potentials declined from 2.02 ± 0.37 mV at 2 weeks to 0.95 ± 0.41 mV at 12 weeks. The amplitude of motor evoked potentials was significantly reduced in a time-dependent manner ($P < 0.05$) (**Figure 4**).

Histological and pathological changes in progressive compression models of SCI
The gross morphology of the spinal cord in the control group remained intact. It had a smooth surface and signs of mild adhesion and bleeding on the dura mater around the drilling site of T_9 lamina. Among the surgery groups, a mild dent on the dorsal medial spinal cord was observed in the spinal cord of mice in the 4-week post-surgery group, part of which was slightly adhered to the lamina. At 8 weeks after surgery, a lateral view of the spinal cord revealed a prominent dorsal indentation (**Figure 5**).

In comparison to the control group, the number of neurons in the anterior (ventral) horn of the compressed seg-

ments in the surgery groups began to decline over time as compression increased. Four weeks after surgery, the number of neurons in ventral horn was normal but gaps appeared in the periphery. The number of vacuoles in parenchymal glial cells had increased. Eight weeks after surgery, the number of neurons had reduced significantly and their cell volumes were relatively small. Their distribution was also disorganized, as evidenced by blurred Nissl bodies (**Figure 6A–D**). Histological micrographs at other time points are not listed because of they are intermediate to adjacent time points.

ChAT immunostaining suggested that in comparison to the control group, the number of ChAT$^+$ neurons in the anterior (ventral) horn of the spinal cord in the surgery groups exhibited a steady decline over time, with increasing oppression. The mean number of neurons in the bilateral anterior horns of the compressed T_9 segment (**Figure 7**) was reduced from 10.80 ± 1.20 in the control group ($n = 6$) to 8.60 ± 0.55 in the 8-week group ($P < 0.05$), then further reduced to 5.00 ± 1.22 in the 12-week group ($P < 0.0001$ *vs.* 8-week group). By 12 weeks post-surgery, only a small number of neurons survived (**Figure 6E–H**).

GFAP immunostaining revealed that astrocytes around the compression site began to exhibit hypertrophic cell bodies and GFAP expression was slightly enhanced after 4 weeks post-surgery, compared with the control group. Astrocytes in the margins of the compression site exhibited significantly increased GFAP expression, disorganized distribution, and local glial scar formation at 8 weeks post-surgery. By 12 weeks, the phenotypes exhibited recovery to levels that were similar to that of 4 weeks after surgery (**Figure 6I–L**).

Iba1 immunostaining revealed that most microglia in the control group were in a resting state, whereas the number of Iba1-positive cells in the 8-week group had significantly increased. These cells contained coarse granules and their shape was noticeably hypertrophic with amoeba-like morphology. This increase in the number and expression of microglial cells is an indication of the cell transformation from a resting to an activated state. With further aggravation of compression, the number of activated microglial cells increased; however, by 12 weeks levels they recovered to numbers similar to those observed 4 weeks after surgery (**Figure 6M–P**).

Discussion
The proportion of SCI patients increased from 7.0% to 14.0% from 2003 to 2011 according to a Chinese study (Yang et al., 2014). Within recent years, global SCI incidence has risen to 83 cases/million people or higher (Hamers et al., 2006; Selassie et al., 2015; Aslam and Fausel, 2016; Knox, 2016; Kristinsdottir et al., 2016; Bárbara-Bataller et al., 2017); however, the social and economic losses are not proportionate to its incidence. Severe disability and death lead to substantial financial and social costs; therefore, SCI has been a focal area of research in spinal surgery and neurosurgery. With the aging population in present-day society, the incidence of degenerative spondylosis caused by spinal stenosis, chronic spinal cord compression, and nerve root disorders has also risen (Neumann et al., 2009). Pathophysiological studies of
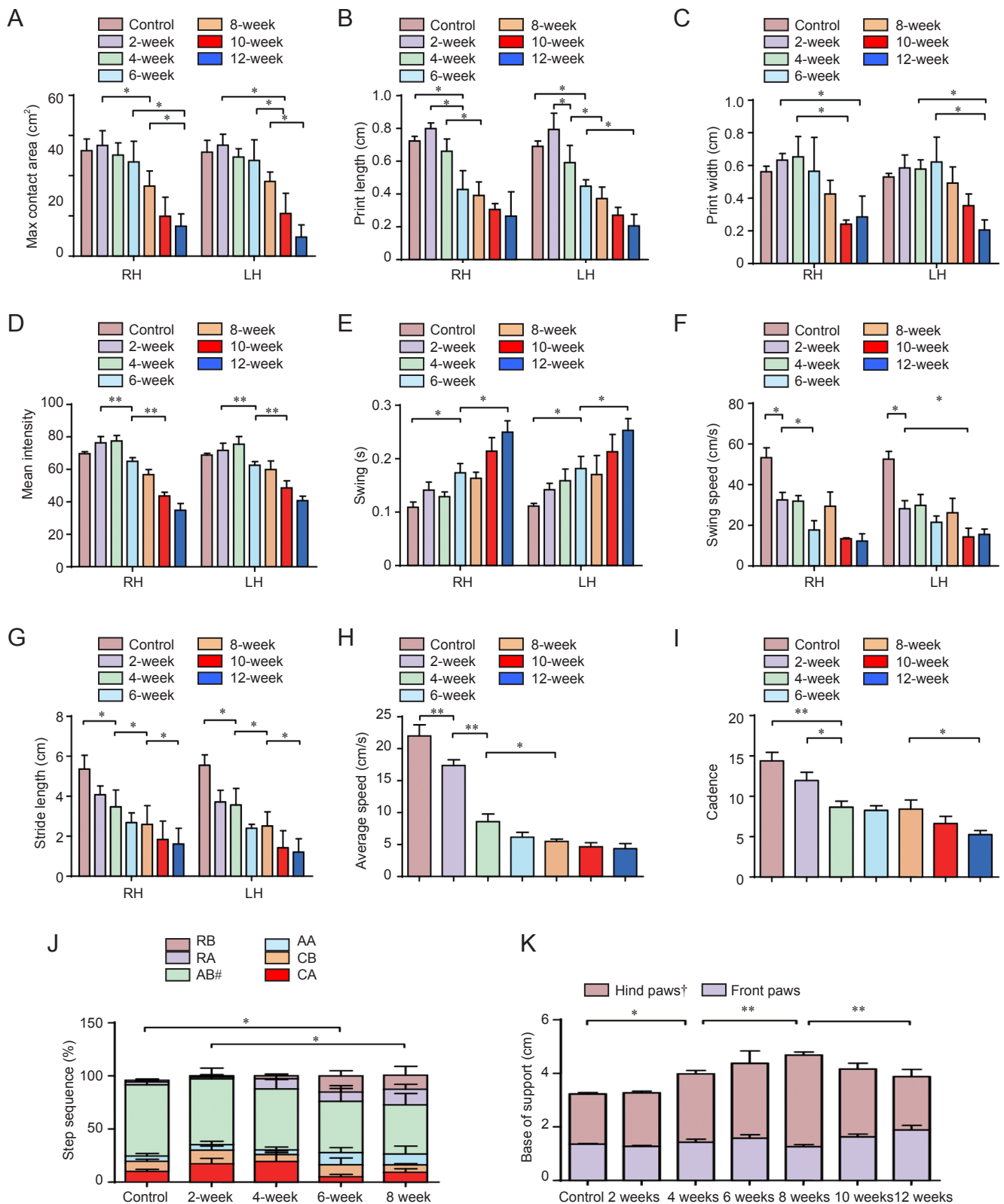
Figure 3 Change of CatWalk-assisted gait analysis in progressive compression models of spinal cord injury.
Gait analysis of mice from each group was conducted using the CatWalk XT automated quantitative gait analysis system. (A–K) Maximum contact area, print length, print width, mean intensity, swing, swing speed, stride length, average speed and cadence, step sequence and base of support, respectively. According to movement sequence of limbs, the step sequence pattern (J) RB to CA respectively refer to: RB: LF-RF-RH-LH; RA: RF-LF-LH-RH; AB: LF-RH-RF-LH; AA: RF-RH-LF-LH; CB: LF-RF-LH-RH; CA: RF-LF-RH-LH; LF: left front; RF: right front; LH: left hind; RH: right hind. Data are expressed as the mean ± SD (n = 6 mice per group), and analyzed by one-way analysis of variance. *$P < 0.05$, **$P < 0.01$. #$P < 0.05$, *vs.* RB, RA, AA, CB, and CA; †$P < 0.05$, *vs.* front paws. Control group: Mice did not receive the injury; 2-, 4-, 6-, 8-, 10-, 12-week groups: after 2, 4, 6, 8, 10, 12 weeks of progressive spinal cord compression injury.
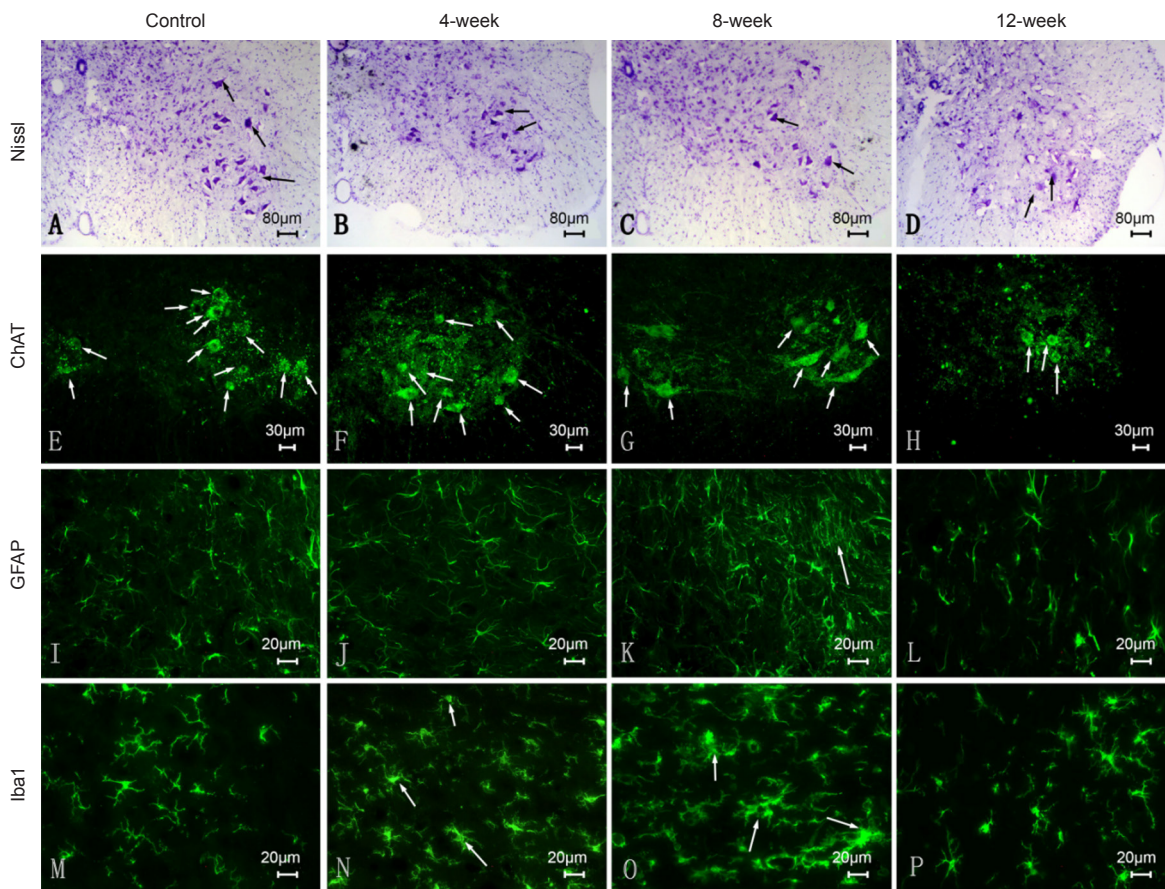
Figure 6 Histological and pathological changes in progressive compression models of spinal cord injury.
(A–D) Nissl staining: Compared to the control group, the number of neurons in the anterior horn of the compressed segments in the surgery groups began to decline over time as compression increased (arrows indicate neurons in ventral horn). (E–H) Choline acetyltransferase (ChAT) immunostaining suggested that compared to the control group, the number of neurons in the anterior horn of the spinal cord in the surgery groups exhibited a steady decline over time, with increasing compression. We chose 1 section located 1 mm distal from compression site of T_9 level for histology (Arrows indicate ChAT+ motor neurons). (I–L) Glial fibrillary acidic protein (GFAP) immunostaining revealed that compared to the control group, as the compression increased, astrocytes around the compression site began to exhibit hypertrophic cell bodies and slightly enhanced expression from 4 weeks post-surgery to 8 weeks post-surgery; by 12 weeks, the phenotypes recovered to levels that were similar to that observed 4 weeks after surgery (arrows indicate activated astrocytes); (M–P) Ionized calcium-binding adapter molecule 1 (Iba1) immunostaining revealed that most microglia in the control group were in a resting state, and the number of Iba1-positive cells in the 8-week group was significantly increased, whereas by 12 weeks, the phenotypes recovered to levels that were similar to that observed 4 weeks post-surgery (arrows indicate activated microglia). Histological micrographs at other time points are not shown because of their similarity with adjacent time points. Control group: Mice did not receive the injury; 4-, 8-, 12-week groups: after 4, 8, 12 weeks of progressive spinal cord compression injury.
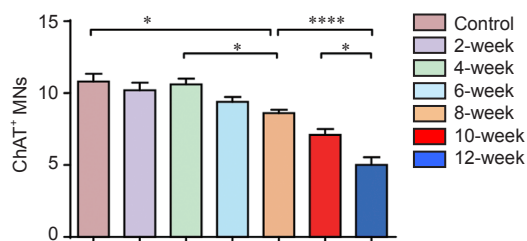
Figure 7 Change of choline acetyltransferase-positive (ChAT+) motor neurons (MNs) in ventral horn in progressive compression models of spinal cord injury.
The mean number of ChAT+ neurons in the bilateral anterior horns of the compressed T_9 segment decreased after 4 weeks post-surgery. Data are expressed as the mean ± SD (n = 6 mice per group), and analyzed by Student-Newman-Keuls test. *$P < 0.05$, ****$P < 0.0001$. Control group: Mice did not receive the injury; 2-, 4-, 6-, 8-, 10-, 12-week groups: after 2, 4, 6, 8, 10, 12 weeks of progressive spinal cord compression injury.

group by 4 weeks post-surgery ($P < 0.05$) (**Figure 3A**, **B**). The maximum contact areas of the left and right hind paws reduced from 0.13 ± 0.03 cm² and 0.13 ± 0.03 cm² in the control group to 0.02 ± 0.03 cm² and 0.04 ± 0.03 cm² in the 12-week group, respectively. The paw print length of the left and right hind paws reduced from 0.58 ± 0.07 cm and 0.60 ± 0.06 cm in the control group to 0.17 ± 0.16 cm and 0.22 ± 0.33 cm in the 12-week group, respectively. The mean intensity increased slightly up to 4 weeks after surgery, then gradually declined (**Figure 3D**). Except for the 2- and 4-week groups, significant differences were also noted between the 2-week and other groups and between 6-week and 10- or 12-week groups ($P < 0.01$).

The mean right hindlimb stride length declined gradually from 4.07 ± 0.45 cm at 2 weeks to 1.61 ± 0.78 cm at 12 weeks (**Figure 3G**). The stride lengths of both hindlimbs differed significantly between the control and 4-week groups, the 4- and 8-week groups, and the 8- and 12-week groups ($P <$

SCI caused by chronic suppression have attracted increasing attention, and SCI models have become critical tools in solving the clinical challenges associated with the condition.

Ideal SCI models should achieve anatomical, histological, behavioral, and even physiological and molecular biological consistency; moreover, the results should be repeatable. As mentioned before, murine models of acute SCI and chronic compression model of rats have been well developed; however, few chronic SCI mouse models are available at present. Models with various injury mechanisms could meet the requirements for research at different levels as it relates to behavior, histology, and molecular biology (Sekhon and Fehlings, 2001). In further research, we will use a variety of gene knockout mice to study aspects of neuroimmunology and metabolism to elucidate the mechanism of chronic spinal cord injury.

In the present study, we established such an experimental chronic compression mouse model of SCI. We found that hindlimb motor dysfunction correlated with the degree of compression of the spinal cord. BMS scores decreased with aggravation of spinal cord compression 8 weeks after surgery. However, after 8 weeks, when there was no further compression, the BMS scores continued to decline. This outcome might be correlated to tissue ischemia caused by prolonged compression, as well as the loss of motor neurons, as confirmed and reviewed by other researchers (Wyndaele and Wyndaele, 2006). So far we had not verified this in our model. Open field actually declined slightly but not significantly; we believe that the front limbs compensate partially for the functional deficiency of the hindlimb. Such changes were reflected in front limb CatWalk data, which are not present in these results because our main focus was hindlimb motor function. As a computer-assisted open-field test, the EthoVision behavioral test can detect spontaneous activities of mice that can be modified by fear, anxiety (Fehlings et al., 2015), and stress aroused by experiments such as pain (Lee-Kubli et al., 2016) and anesthesia. We found that the mouse model does not exhibit a significant reduction in spontaneous activities following surgical compression, which makes any behavioral changes even more significant.

CatWalk-assisted gait analysis of chronic SCI has been reported (Datto et al., 2015; Forner et al., 2016; Kang et al., 2016). In the present study, the maximum contact areas of the hind paws declined gradually. This consequence is not consistent with those of other studies on mouse transection and contusion models of SCI (Hefner and Holmes, 2007). The swing is both relatively sensitive to speed, and independent of speed. Previous studies have suggested that in acute SCI models, the swing is shortened within 3 weeks, but then increases 4 weeks post-surgery (Hefner and Holmes, 2007). This is consistent with the results of the present study at 4 weeks. However, some studies have reported a steady increase in swing following injury (Pham et al., 2009), so more studies are needed to resolve such differences. The base of support measurements in the present study gradually increased after 8 weeks, along with an increasingly unsteady gait. These are consistent with the findings of previous studies (Hefner and Holmes, 2007). However, the reason for the gradual decline after 8 weeks requires further study.

The stride length of the hind paws was reduced; this finding is similar to that of the contusion model of acute SCI, but different from that of the dorsal transection model of SCI (Hefner and Holmes, 2007). The frequency of the regular step sequence in mice with spinal cord compression showed a reduction, and that of an abnormal gait showed a relative increase (Hasnie et al., 2007). The maximum contact areas of bilateral front paws and the paw print width increased with aggravation of the spinal cord compression; however, no significant differences were noted between groups. In contrast, the swing and stride length of front paws both exhibited a shortening trend. This change in stride length of the front paws was similar to that of the hind paws; however, other related parameters exhibited no specific patterns. We found that the histological properties of the spinal cord in this model correlated with the degree of compression. Nissl and ChAT staining confirmed that the number of neurons in the anterior (ventral) horns gradually declined before 8 weeks, with only a minority remaining by 12 weeks. This interval is consistent with the time around which the number of neurons decline in a rat model of chronic compression of the thoracic spinal cord (Cheng et al., 1997). Currently, it is accepted that activated astrocytes play a role in axonal repair and promote functional recovery of nerves following SCI (Klapka et al., 2005; Hendriks et al., 2006). Since progressive screw compression for up to 8 weeks simulated sustained constriction injury, GFAP staining suggests that the period of astrocyte activation correlated with that of a continual increase in compression. This finding is consistent with a previous report on constriction injuries (Hendriks et al., 2006).

Microglia, inflammatory cells in the central nervous system, play important roles in immunity (Faulkner et al., 2004; Kasahara et al., 2006), cytotoxicity (Davies et al., 2011), and repair (Wirenfeldt et al., 2011). Iba1 staining showed that the timing of microglia activation was consistent with that of progressive compression. Although motor dysfunction of the hindlimbs continued to worsen after 8 weeks, by 12 weeks, microglial cells exhibited less reactivity than before. Reports regarding the reactivity of microglia subjected to prolonged compression are lacking, whereas those in brain research confirmed that necrosis results in a glial scar (Boltze et al., 2012; Qin et al., 2015). Furthermore, locomotor dysfunction is apparently not associated with the detrimental effects of microglial activation, but might be associated with the significant reduction of motor neurons in the anterior (ventral) horn, spinal cord ischemia, and demyelination (Aloisi, 2001). In our future research, we plan to explore changes in the inflammatory cytokine profile, after perfecting this chronic compression model of SCI, as well as its relationship with the chronic pathological changes of the spinal cord and neurological function.

By combining repeatable motor function evaluations and histological observations, we successfully generated a progressive flat-head screw compression mouse model of thoracic SCI. This model is simple and reproducible. Considering the volume of the spinal canal in the mouse and the thickness of the lamina, we used a flat-head screw to replace the general expandable material (Kurokawa et al., 2011), spacer (Dimar

et al., 1999), and balloon (Kasahara et al., 2006) techniques previously utilized to simulate epidural oppression. We quantitatively controlled the depth of compression in the spinal canal by screwing in a specific number of turns. CatWalk-assisted gait analysis demonstrated the consistency between the degree of spinal cord compression and that of locomotor dysfunction in the hindlimbs. Although a microscope was used during surgery to increase the accuracy of placing the relevant devices and a stereotaxic instrument was used to fix the cranial microdrill and prevent interference with the spinal cord during drilling process, there were losses of subjects (2/42) from acute SCI during surgery or loosening and displacement of the implanted screw (3/36). Despite administration of antibiotics to prevent infection post-surgery, 2/42 animals were lost to serious infections. These animals had to be excluded and replaced. To prevent surgical failure and postoperative complications, refined surgical procedures, good postoperative care, and regular monitoring are required. We regularly observed voiding and bladder filling throughout the study. Although micturition and bladder function were not quantified, that might be worth including in future studies.

In the present mouse model, progressively increasing screw compression in each experimental group induced different types of SCI. The present study therefore provides preliminary exploration of the feasibility and reproducibility of the progressive screw compression model of SCI in mice. Since our histological study and gait analysis of mice yielded different degrees of compression at the same interval, or similar degrees of compression at different intervals, further study is necessary.

In summary, the experiment successfully established a progressive compressive thoracic SCI model in mice that is reproducible, simple, and practical, which can simulate posterior epidural spinal cord compression. Evaluation of motor function and histopathological observations suggest that the degree of compression by screw is associated with locomotor dysfunction and spinal cord tissue damage in experimental animals. These make it a preferred chronic compression SCI model in mice. This novel mouse model of chronic spinal cord compression provides a reliable basis for further basic and clinical studies on chronic SCI.

Additional file: *Additional Figure 1 Flat-head screw was implanted to establish a model of thoracic spinal cord progressive compression mouse*

References

Aloisi F (2001) Immune function of microglia. Glia 36:165-179.

Aslam H, Fausel ZC (2016) Epidemiology of fractures in men with spinal cord injury. PM R 8:S154.

Bárbara-Bataller E, Méndez-Suárez JL, Alemán-Sánchez C, Ramírez-Lorenzo T, Sosa-Henríquez M (2017) Epidemiology of traumatic spinal cord injury in Gran Canaria. Neurocirugia (Astur) 28:15-21.

Basso DM, Fisher LC, Anderson AJ, Jakeman LB, McTigue DM, Popovich PG (2006) Basso Mouse Scale for locomotion detects differences in recovery after spinal cord injury in five common mouse strains. J Neurotrauma 23:635-659.

Boltze J, Schmidt UR, Reich DM, Kranz A, Reymann KG, Strassburger M, Lobsien D, Wagner DC, Forschler A, Schabitz WR (2012) Determination of the therapeutic time window for human umbilical cord blood mononuclear cell transplantation following experimental stroke in rats. Cell Transplant 21:1199-1211.

Chagas H, Domingues F, Aversa A, Vidal Fonseca AL, de Souza JM (2005) Cervical spondylotic myelopathy: 10 years of prospective outcome analysis of anterior decompression and fusion. Surg Neurol 64 Suppl 1:S1:30-35; discussion S1:35-36.

Cheng H, Almstrom S, Gimenez-Llort L, Chang R, Ove Ogren S, Hoffer B, Olson L (1997) Gait analysis of adult paraplegic rats after spinal cord repair. Exp Neurol 148:544-557.

Cheriyan T, Ryan DJ, Weinreb JH, Cheriyan J, Paul JC, Lafage V, Kirsch T, Errico TJ (2014) Spinal cord injury models: a review. Spinal Cord 52:588-595.

Datto JP, Bastidas JC, Miller NL, Shah AK, Arheart KL, Marcillo AE, Dietrich WD, Pearse DD (2015) Female rats demonstrate improved locomotor recovery and greater preservation of white and gray matter after traumatic spinal cord injury compared to males. J Neurotrauma 32:1146-1157.

Davies SJ, Shih CH, Noble M, Mayer-Proschel M, Davies JE, Proschel C (2011) Transplantation of specific human astrocytes promotes functional recovery after spinal cord injury. PLoS One 6:e17328.

Dimar JR, 2nd, Glassman SD, Raque GH, Zhang YP, Shields CB (1999) The influence of spinal canal narrowing and timing of decompression on neurologic recovery after spinal cord contusion in a rat model. Spine (Phila Pa 1976) 24:1623-1633.

Ding Y, Qu Y, Feng J, Wang M, Han Q, So KF, Wu W, Zhou L (2014) Functional motor recovery from motoneuron axotomy is compromised in mice with defective corticospinal projections. PLoS One 9:e101918.

Faulkner JR, Herrmann JE, Woo MJ, Tansey KE, Doan NB, Sofroniew MV (2004) Reactive astrocytes protect tissue and preserve function after spinal cord injury. J Neurosci 24:2143-2155.

Fehlings MG (2009) The impact of continued cord compression following traumatic spinal cord injury. J Neurosurg Spine 11:568-569; discussion 569.

Fehlings MG, Tetreault L, Nater A, Choma T, Harrop J, Mroz T, Santaguida C, Smith JS (2015) The aging of the global population: the changing epidemiology of disease and spinal disorders. Neurosurgery 77 Suppl 4:S1-5.

Fonseca AF, Scheffer JP, Coelho BP, Aiello G, Guimaraes AG, Gama CR, Vescovini V, Cabral PG, Oliveira AL (2016) Technique of spinal cord compression induced by inflation of epidural balloon catheter in rabbits (Oryctologus cuniculus): efficient and easy to use model. An Acad Bras Cienc 88:1511-1517.

Forner S, Martini AC, de Andrade EL, Rae GA (2016) Neuropathic pain induced by spinal cord injury: Role of endothelin ETA and ETB receptors. Neurosci Lett 617:14-21.

Hamers FP, Koopmans GC, Joosten EA (2006) CatWalk-assisted gait analysis in the assessment of spinal cord injury. J Neurotrauma 23:537-548.

Han Q, Cao C, Ding Y, So KF, Wu W, Qu Y, Zhou L (2015) Plasticity of motor network and function in the absence of corticospinal projection. Exp Neurol 267:194-208.

Hasnie FS, Wallace VC, Hefner K, Holmes A, Rice AS (2007) Mechanical and cold hypersensitivity in nerve-injured C57BL/6J mice is not associated with fear-avoidance- and depression-related behaviour. Br J Anaesth 98:816-822.

Hautier L, Charles C, Asher RJ, Gaunt SJ (2014) Ossification sequence and genetic patterning in the mouse axial skeleton. J Exp Zool B Mol Dev Evol 322:631-642.

Hefner K, Holmes A (2007) Ontogeny of fear-, anxiety- and depression-related behavior across adolescence in C57BL/6J mice. Behav Brain Res 176:210-215.

Hendriks WT, Eggers R, Ruitenberg MJ, Blits B, Hamers FP, Verhaagen J, Boer GJ (2006) Profound differences in spontaneous long-term functional recovery after defined spinal tract lesions in the rat. J Neurotrauma 23:18-35.

Hol EM, Pekny M (2015) Glial fibrillary acidic protein (GFAP) and the astrocyte intermediate filament system in diseases of the central nervous system. Curr Opin Cell Biol 32:121-130.

Kalsi-Ryan S, Karadimas SK, Fehlings MG (2013) Cervical spondylotic myelopathy: the clinical phenomenon and the current pathobiology of an increasingly prevalent and devastating disorder. Neuroscientist 19:409-421.

Kang DW, Moon JY, Choi JG, Kang SY, Ryu Y, Park JB, Lee JH, Kim HW (2016) Antinociceptive profile of levo-tetrahydropalmatine in acute and chronic pain mice models: role of spinal sigma-1 receptor. Sci Rep 6:37850.

Karadimas SK, Gialeli CH, Klironomos G, Tzanakakis GN, Panagiotopoulos E, Karamanos NK, Gatzounis G (2010) The role of oligodendrocytes in the molecular pathobiology and potential molecular treatment of cervical spondylotic myelopathy. Curr Med Chem 17:1048-1058.

Karadimas SK, Moon ES, Yu WR, Satkunendrarajah K, Kallitsis JK, Gatzounis G, Fehlings MG (2013) A novel experimental model of cervical spondylotic myelopathy (CSM) to facilitate translational research. Neurobiol Dis 54:43-58.

Kasahara K, Nakagawa T, Kubota T (2006) Neuronal loss and expression of neurotrophic factors in a model of rat chronic compressive spinal cord injury. Spine (Phila Pa 1976) 31:2059-2066.

Klapka N, Hermanns S, Straten G, Masanneck C, Duis S, Hamers FP, Muller D, Zuschratter W, Muller HW (2005) Suppression of fibrous scarring in spinal cord injury of rat promotes long-distance regeneration of corticospinal tract axons, rescue of primary motoneurons in somatosensory cortex and significant functional recovery. Eur J Neurosci 22:3047-3058.

Knox J (2016) Epidemiology of spinal cord injury without radiographic abnormality in children: a nationwide perspective. J Child Orthop 10:255-260.

Kristinsdottir EA, Knutsdottir S, Sigvaldason K, Jonsson H, Jr., Ingvarsson PE (2016) Epidemiology of spinal cord injury in Iceland from 1975 to 2014. Laeknabladid 102:491-496.

Kurokawa R, Murata H, Ogino M, Ueki K, Kim P (2011) Altered blood flow distribution in the rat spinal cord under chronic compression. Spine (Phila Pa 1976) 36:1006-1009.

Lee-Kubli CA, Ingves M, Henry KW, Shiao R, Collyer E, Tuszynski MH, Campana WM (2016) Analysis of the behavioral, cellular and molecular characteristics of pain in severe rodent spinal cord injury. Exp Neurol 278:91-104.

Li GL, Farooque M, Isaksson J, Olsson Y (2004) Changes in synapses and axons demonstrated by synaptophysin immunohistochemistry following spinal cord compression trauma in the rat and mouse. Biomed Environ Sci 17:281-290.

Li XQ, Wang J, Fang B, Tan WF, Ma H (2014) Intrathecal antagonism of microglial TLR4 reduces inflammatory damage to blood-spinal cord barrier following ischemia/reperfusion injury in rats. Mol Brain 7:28.

Manabe S, Ohno T, Tanaka H, Park P (1988) Spinal cord compression by epidural metastases. Fibrosarcoma experiments in rats. Acta Orthop Scand 59:117-121.

Nashmi R, Fehlings MG (2001) Changes in axonal physiology and morphology after chronic compressive injury of the rat thoracic spinal cord. Neuroscience 104:235-251.

Neumann M, Wang Y, Kim S, Hong SM, Jeng L, Bilgen M, Liu J (2009) Assessing gait impairment following experimental traumatic brain injury in mice. J Neurosci Methods 176:34-44.

Noldus LP, Spink AJ, Tegelenbosch RA (2001) EthoVision: a versatile video tracking system for automation of behavioral experiments. Behav Res Methods Instrum Comput 33:398-414.

Perdiki M, Farooque M, Holtz A, Li GL, Olsson Y (1998) Expression of endothelial barrier antigen immunoreactivity in blood vessels following compression trauma to rat spinal cord. Temporal evolution and relation to the degree of the impact. Acta Neuropathol 96:8-12.

Pham J, Cabrera SM, Sanchis-Segura C, Wood MA (2009) Automated scoring of fear-related behavior using EthoVision software. J Neurosci Methods 178:323-326.

Qin J, Ma X, Qi H, Song B, Wang Y, Wen X, Wang QM, Sun S, Li Y, Zhang R, Liu X, Hou H, Gong G, Xu Y (2015) Transplantation of induced pluripotent stem cells alleviates cerebral inflammation and neural damage in hemorrhagic stroke. PLoS One 10:e0129881.

Rades D, Janssen S, Kasmann L, Bolm L, Schild SE (2016) Outcomes after irradiation of epidural spinal cord compression due to metastatic thyroid cancer. Anticancer Res 36:2035-2039.

Rajah G, To CY, Sood S, Ham S, Altinok D, Poulik J, Haridas A (2014) Epidural spinal cord compression in a patient with blue rubber bleb nevus syndrome. J Neurosurg Pediatr 14:486-489.

Scivoletto G, Tamburella F, Laurenza L, Torre M, Molinari M (2014) Who is going to walk? A review of the factors influencing walking recovery after spinal cord injury. Front Hum Neurosci 8:141.

Sekhon LH, Fehlings MG (2001) Epidemiology, demographics, and pathophysiology of acute spinal cord injury. Spine (Phila Pa 1976) 26:S2-12.

Selassie A, Cao Y, Saunders LL (2015) Epidemiology of traumatic spinal cord injury among persons older than 21 years: a population-based study in south Carolina, 1998-2012. Top Spinal Cord Inj Rehabi21:333-344.

Tatsui CE, Lee SH, Amini B, Rao G, Suki D, Oro M, Brown PD, Ghia AJ, Bhavsar S, Popat K, Rhines LD, Stafford RJ, Li J (2016) Spinal laser interstitial thermal therapy: a novel alternative to surgery for metastatic epidural spinal cord compression. Neurosurgery 79 Suppl 1:S73-82.

Uchida K, Nakajima H, Sato R, Kokubo Y, Yayama T, Kobayashi S, Baba H (2005) Multivariate analysis of the neurological outcome of surgery for cervical compressive myelopathy. J Orthop Sci 10:564-573.

Watanabe N, Sugimoto Y, Tanaka M, Mazaki T, Arataki S, Takigawa T, Kataoka M, Kunisada T, Ozaki T (2016) Neurological recovery after posterior spinal surgery in patients with metastatic epidural spinal cord compression. Acta Med Okayama 70:449-453.

Weaver LC, Verghese P, Bruce JC, Fehlings MG, Krenz NR, Marsh DR (2001) Autonomic dysreflexia and primary afferent sprouting after clip-compression injury of the rat spinal cord. J Neurotrauma 18:1107-1119.

Wirenfeldt M, Babcock AA, Vinters HV (2011) Microglia - insights into immune system structure, function, and reactivity in the central nervous system. Histol Histopathol 26:519-530.

Wyndaele M, Wyndaele JJ (2006) Incidence, prevalence and epidemiology of spinal cord injury: what learns a worldwide literature survey? Spinal Cord 44:523-529.

Yang R, Guo L, Wang P, Huang L, Tang Y, Wang W, Chen K, Ye J, Lu C, Wu Y, Shen H (2014) Epidemiology of spinal cord injuries and risk factors for complete injuries in Guangdong, China: a retrospective study. PLoS One 9:e84733.

Young W (2002) Spinal cord contusion models. Prog Brain Res 137:231-255.

Ziu M, Fletcher L, Savage JG, Jimenez DF, Digicaylioglu M, Bartanusz V (2014) Spatial and temporal expression levels of specific microRNAs in a spinal cord injury mouse model and their relationship to the duration of compression. Spine J 14:353-360.